ICES Journal of
Marine Science

The impact of ocean acidification and warming on the skeletal mechanical properties of the sea urchin *Paracentrotus lividus* from laboratory and field observations

Marie Collard[1,2]*, Samuel P. S. Rastrick[3,4], Piero Calosi[3,5], Yoann Demolder[1], Jean Dille[6], Helen S. Findlay[7], Jason Michael Hall-Spencer[3], Marco Milazzo[8], Laure Moulin[1,9], Steve Widdicombe[3], Frank Dehairs[2], and Philippe Dubois[1]

[1]Laboratoire de Biologie Marine, Université Libre de Bruxelles, 50 Avenue F.D. Roosevelt, Brussels B-1050, Belgium

[2]Laboratory for Analytical, Environmental and Geo-Chemistry, Earth Systems Science Research Group, Vrije Universiteit Brussel, Pleinlaan 2, Brussels 1050, Belgium

[3]Marine Biology and Ecology Research Centre, Plymouth University, Plymouth PL4 8AA, UK

[4]Marine Invertebrate Physiology and Immunology Ocean and Earth Science, National Oceanography Centre Southampton, University of Southampton Waterfront Campus, European Way, Southampton SO14 3ZE, UK

[5]Département de Biologie, Chimie et Géographie, Université du Québec à Rimouski, 300 Allée des Ursulines, Rimouski, QC, Canada G5L 3A1

[6]4MAT Department, Université Libre de Bruxelles, 50 Avenue F.D. Roosevelt, Brussels B-1050, Belgium

[7]Plymouth Marine Laboratory, Prospect Place, West Hoe, Plymouth PL1 3 DH, UK

[8]Dipartimento di Scienze della Terra e del Mare, Università di Palermo, Via Archirafi, 28, Palermo, Italy

[9]Laboratoire d'Ecologie Numérique des Milieux Aquatiques, Université de Mons-Hainaut, 23 Place du Parc, Mons B-7000, Belgium

*Corresponding author: tel: +32 2 650 29 70; fax: +32 2 650 27 96; e-mail: marie.collard9@gmail.com

Increased atmospheric CO_2 concentration is leading to changes in the carbonate chemistry and the temperature of the ocean. The impact of these processes on marine organisms will depend on their ability to cope with those changes, particularly the maintenance of calcium carbonate structures. Both a laboratory experiment (long-term exposure to decreased pH and increased temperature) and collections of individuals from natural environments characterized by low pH levels (individuals from intertidal pools and around a CO_2 seep) were here coupled to comprehensively study the impact of near-future conditions of pH and temperature on the mechanical properties of the skeleton of the euechinoid sea urchin *Paracentrotus lividus*. To assess skeletal mechanical properties, we characterized the fracture force, Young's modulus, second moment of area, material nanohardness, and specific Young's modulus of sea urchin test plates. None of these parameters were significantly affected by low pH and/or increased temperature in the laboratory experiment and by low pH only in the individuals chronically exposed to lowered pH from the CO_2 seeps. In tidal pools, the fracture force was higher and the Young's modulus lower in ambital plates of individuals from the rock pool characterized by the largest pH variations but also a dominance of calcifying algae, which might explain some of the variation. Thus, decreases of pH to levels expected for 2100 did not directly alter the mechanical properties of the test of *P. lividus*. Since the maintenance of test integrity is a question of survival for sea urchins and since weakened tests would increase the sea urchins' risk of predation, our findings indicate that the decreasing seawater pH and increasing seawater temperature expected for the end of the century should not represent an immediate threat to sea urchins vulnerability.

Keywords: CO_2 seep, intertidal pools, long-term exposure, mechanical properties, ocean acidification, *Paracentrotus lividus*, sea urchin, skeleton.

Introduction

The atmospheric carbon dioxide (CO_2) concentration has increased from 280 to 400 ppm due to anthropogenic activities such as fossil fuel burning (IPCC, 2013). The continually increasing concentration of atmospheric CO_2 is leading to an increase in the mean global seawater temperature, which is expected to be 2°C warmer by the end of this century, and is changing seawater carbonate chemistry as CO_2 dissolves into the surface waters (decreasing pH and carbonate ions concentration; Caldeira and Wickett, 2003; Sokolov et al., 2009; Orr, 2011). A reduction in carbonate ions results in a decreased saturation state (Ω) of seawater for carbonate calcium minerals. Such minerals are built by several marine organisms, including echinoderms which produce high-magnesium calcite, one of the most soluble forms of calcium carbonate (Morse et al., 2006).

Changes in the ocean carbonate chemistry have been indicated to have potential negative effects on the integrity of calcifying marine organisms' skeleton. As previously shown for crustaceans, coccolithophores, and molluscs, calcification may be impaired and calcium carbonate skeletons may dissolve (e.g. McDonald et al., 2009; Welladsen et al., 2010; Ziveri et al., 2014). Although some organisms upregulate calcification rates as carbonate saturation states fall, unprotected skeletons and shells dissolve once Ω falls below 1 (Rodolfo-Metalpa et al., 2011). Thus, in general, the mechanical properties of skeletons could be affected as Ω falls (McDonald et al., 2009; Welladsen et al., 2010). Sea urchin skeletons are of basic importance in defining the organism structure, providing protection against hydrodynamic forces and predators, and enabling locomotion and food gathering. Consequently, any deterioration of the skeleton would have considerable consequences on the sea urchin fitness. However, sea urchins thrive in naturally undersaturated waters such as upwelling zones where pH may reach values of 7.75, tidal pools where during nocturnal low tide pH can decrease to 7.4, around CO_2 seep in areas with pH 7.4, in deep ocean, and in Antarctic waters where the $CaCO_3$ saturation state is below 1 (e.g. David et al., 2005; Hall-Spencer et al., 2008; Moulin et al., 2011; LaVigne et al., 2013; Collard et al., 2014a; Dery et al., 2014).

In adult sea urchins, the skeleton is embedded within the dermis which is itself covered by the epidermis (except for the particular case of the cidaroid sea urchins' spines which lack a covering epidermis; Dery et al., 2014). The skeleton is principally composed of the test, encompassing the body, the spines (Figure 1), and the chewing

Figure 1. Aboral view of the test of an euechinoid and illustration of the plates sampled for the mechanical tests (adapted from Trousset, 1885).

apparatus, called Aristotle's lantern. The different ossicles of the skeleton are made of a three-dimensional network of calcium carbonate trabeculae called the stereom which has pores filled with connective tissue, the stroma (Dubois and Chen, 1989). The test plates are almost never fused but are tightly held against each other by ligaments rolled around the outermost trabeculae and the trabeculae from one plate are inserted within the pores of the adjacent plates (Ellers et al., 1998). The main calcium carbonate mineral formed by adult sea urchins is high-magnesium calcite, one of the most soluble forms of calcite (Morse et al., 2006). However, calcification takes place intracellularly, within closed syncytia, and therefore the skeleton is almost never in contact with seawater (Dubois and Chen, 1989). Indirectly, calcification could be impacted by the cost of maintaining acid–base balance, i.e. removing protons and CO_2 that are produced during the calcification process. Indeed, the cost of maintaining homeostasis across a natural pH gradient can affect the distribution of marine invertebrates (Calosi et al., 2013a). The elimination of protons into the extracellular fluids will have an increased energetic cost if the concentration of protons within these fluids is also elevated by acidosis due to lower pH seawater, as shown in the gastropod *Littorina littorea* (Melatunan et al., 2013). Some sea urchin species appear able to partly or fully compensate extracellular pH (Stumpp et al., 2012; Collard et al., 2013, 2014b; Moulin et al., 2014) including across natural pH gradients (Calosi et al., 2013a). Others appear unable to do so (Kurihara et al., 2013) and some species show naturally a low coelomic fluid pH, and an undersaturation towards high-magnesium calcite (pH 7.1, $\Omega_{Ar} < 1$; Calosi et al., 2013b; Collard et al., 2013, 2014a, b).

Mechanical properties can be affected through different processes. Changes in the growth rate may affect the three-dimensional morphology or density of the stereom (Smith, 1980), which will result in modified mechanical properties (e.g. Moureaux et al., 2010). Alternatively, the structural properties of the material itself may be affected by the formation of imperfections during the $CaCO_3$ precipitation (e.g. Moureaux et al., 2011). For these reasons, different mechanical tests should be applied to fully describe the mechanical properties. Bending and compression tests measure the structural properties and how a change in the shape and/or the repartition of the material within the skeletal piece may affect its overall strength. Complementarily, nanoindentation measures the strength of the material itself as it is applied to a very small surface. Using both types of measurements may disentangle the question of knowing if it is the shape that is affected or the material.

Most studies carried out on ocean acidification impacts on sea urchin skeletons concern growth (for a review, see Dubois, 2014). Several studies reported reduced growth rates of the test and/or spines, especially in juveniles; while other studies showed no effect of the same conditions on these rates (Dubois, 2014). The studies investigating the impact of temperature on sea urchin skeleton have also focused on growth rates showing either no impact or enhanced growth when temperature is increased (e.g. Hermans et al., 2010; Wolfe et al., 2013). Very few studies have addressed the impact of seawater acidification on mechanical properties of the skeleton, and none investigated the impact of temperature (e.g. Asnaghi et al., 2013; Holtmann et al., 2013). However, the methods used in those studies presented bias resulting in difficultly interpretable data (Ellers et al., 1998; Dubois, 2014). More importantly, all the aforementioned studies have investigated the effects of ocean acidification after short-term exposures (<6 months), but recent studies have shown that long-term exposures (≥ 1 year) may allow
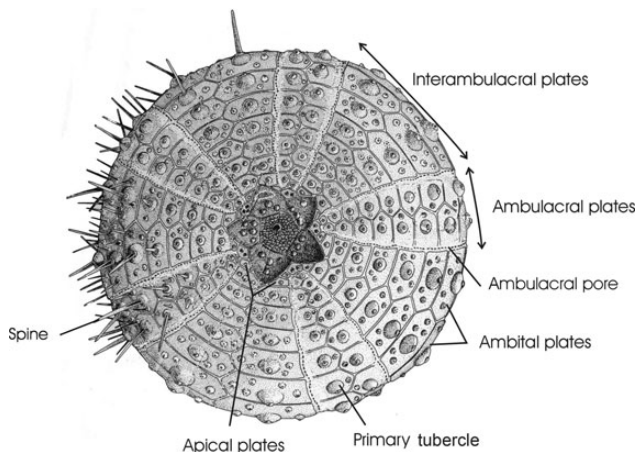
for the acclimatization of sea urchins to acidified conditions. In particular, Dupont *et al.* (2013) showed that after 12 months of exposure the negative effects of reduced seawater pH observed during short-term exposure do not apply anymore. Furthermore, previous studies have used analogue open systems for future ocean conditions such as CO_2 seeps or intertidal pools to study the impact of reduced pH exposure on sea urchins (e.g. Hall-Spencer *et al.*, 2008; Calosi *et al.*, 2013b) but none of them focused on skeletal mechanical properties of sea urchins.

The goal of the present study was to comprehensively assess the impact of changes in seawater pH and temperature on the skeletal mechanical properties of the sea urchin *Paracentrotus lividus* (Lamarck, 1816), in both a laboratory experiment and in the field. First, we investigated the effect of long-term (12 months) laboratory exposure to decreased pH (8.0 as control, 7.9 and 7.8) and increased temperature ($+2°C$). Second, we investigated the effect of natural acclimatization/adaptation in intertidal pools where individuals are intermittently exposed to pH changes (of up to 0.5 pH units during a single tide) and chronically exposed to natural pH levels along a gradient (pH 8.2–7.7) at CO_2 seeps off Vulcano Island, Italy. We applied several mechanical tests including compression, three-point bending, and nanoindentation tests (Ellers *et al.*, 1998; Moureaux *et al.*, 2011) to evaluate the effect of ocean acidification on whole-organism structural strength and individual plate (ambital and apical) properties.

Material and methods
Plate sampling
All measurements were carried out on skeletons of adult individuals of the sea urchin *P. lividus*. The sea urchin test is composed of individual plates held together by tissue. On those plates, the spines are articulated on the tubercles. The plates are arranged in five interambulacral and five ambulacral double rows (Figure 1). We used inter-ambulacral plates for all mechanical tests rather than the ambulacral plates, since the latter result from the fusion of 2–3 platelets and are pierced with pores for the extrusion of the tube feet, rendering calculations of mechanical properties particularly complex (Smith, 1980). We used two types of interambulacral plates: the apical plates, i.e. the uppermost plates which are the most recently added and the smallest plates, and the ambital plates, i.e. middle plates which are the largest and are located along the ambitus (the largest diameter) of the sea urchin (Deutler, 1926; Figure 1). Samples were collected by dissecting along an ambulacral row from the peristomial membrane to ~1 cm from the apical disc, from there, they were cut horizontally across two interambulacral rows and down to the peristomial membrane again along an ambulacral row. This avoided any damage to the interambulacral ambital and apical plates.

Twelve-month laboratory acclimation
The effects of long-term exposure to elevated temperature and reduced pH conditions predicted to occur by the end of this century (Caldeira and Wickett, 2003; Sokolov *et al.*, 2009; Orr, 2011) on skeletal structures of adult *P. lividus* (supplied by Dunmanus Seafoods Ltd, Durrus, Bantry, Co. Cork, Ireland) were assessed by conducting a 49 weeks long mesocosm experiment at the Plymouth Marine Laboratory (PML, Plymouth, UK) from March 2011 to February 2012 (same system as Findlay *et al.*, 2013, and Queiros *et al.*, 2014). Five nominal treatments were used: "present" [380 µatm (pH 8.0) and seasonal temperature cycle,

380A]; "elevated pCO_2" [750 µatm (pH 7.9) and seasonal temperature cycle, 750A]; "extreme elevated pCO_2" [1000 µatm (pH 7.8) and seasonal temperature cycle, 1000A]; "elevated temperature" [380 µatm (pH 8.0) and 2°C added to the seasonal temperature cycle, 380A+2]; and "combined" [750 µatm (pH 7.9) and 2°C added to the seasonal temperature cycle, 750A+2]. Present day pCO_2 conditions of 380 µatm were maintained by bubbling untreated air, whereas higher pCO_2 treatments were bubbled with enriched-CO_2 air (after, Findlay *et al.*, 2008). Temperature was maintained by the use of heaters and chillers and monthly adjustments were made to reproduce the natural seasonal variations. pCO_2 and temperature were maintained separately in each aquarium. The photoperiod was also adjusted monthly to that of the natural conditions (winter L:D period 8.5 h:15.5 h, summer L:D period 16.5 h:7.5 h). Each nominal treatment was replicated four times and sea urchins randomly assigned to the four aquaria (1 m^3). Within each aquarium, the sea urchins were further divided into individual boxes pierced with holes for water circulation. Water quality was assessed by weekly measurements of nitrate levels (Bran+Luebbe Ltd AAIII, Seal Analytical, Mecquon, WI, USA), and when the concentration reached 25 mg l^{-1}, a third of the seawater volume was changed (in addition to the standard 1/3 volume change done every 3 weeks for all aquaria). The mean ($\pm$ s.d.) nitrate concentration was 3.7 ± 11.1 (range: 0.02–78.85 µmol l^{-1}). Sea urchins were fed with macroalgae (*Ulva lactuca* and *Laminaria* sp.) collected from Plymouth Sound once a week for 48 h. Excessive food and faecal pellets were removed after feeding.

Seawater used for our experimental system was collected from PML's long-term monitoring site "L4" in the Western English Channel (50°15.00′N 4°13.02′W; L4, Western Channel Observatory; for seasonal data on carbon cycle, see Kitidis *et al.*, 2012). Seawater physicochemical parameters were measured three times a week. All methods and data are available online from Findlay *et al.* (2013). Carbonate system parameters that were not directly measured were calculated from temperature, salinity, pH, and A_T as described in Findlay *et al.* (2013). Water chemistry parameters are presented in Table 1.

Sea urchins employed for mechanical tests were sampled from all four replicate aquaria for each treatment after 12 months of exposure, dissected, cleaned of internal organs, and dried for 48 h at 50°C: $n = 10$ for 380A, 11 for 750A+2, and 12 for 750A, 1000A, and 380A+2. The mean diameter at the ambitus (mean $\pm$ s.d.) was 39.9 ± 5.4, 41.4 ± 3.7, 38.8 ± 4.5, 40.6 ± 3.2, and 41.9 ± 6.4 mm for treatments 380A, 750A, 1000A, 380A+2, and 750A+2, respectively. Three ambital interambulacral plates and three apical interambulacral plates per sea urchin were used for mechanical tests. Also, three plates of each type were taken from three individuals per treatment (from different aquaria) for nanoindentation measurements.

Intertidal pools
The effect of intermittent exposure to low pH was investigated by collecting sea urchins in intertidal pools in Crozon (Brittany, France) in February 2013. They were taken from three intertidal rock pools previously characterized (Moulin *et al.*, 2011) and showing different pH regimes during low tide. Seawater in tide pool A was characterized by moderate pH variation during a night tide (-0.2 pH units), tide pool C showed the largest pH changes (-0.5 pH units), and tide pool B was intermediate (-0.4 pH

Table 1. Mean water and carbonate system parameters (mean ± s.d.) for the different treatments of the laboratory experiment per 3-month periods.

	Time point (months)	A_T (µmol kg$_{SW}^{-1}$)	pH$_{NBS}$	Temp (°C)	Salinity	DIC (µmol kg$_{SW}^{-1}$)	pCO$_2$ (µatm)	Ω Ca	Ω Ar
380 A	0–3	2131.0 ± 0.0	8.02 ± 0.09	10.49 ± 0.71	34.3 ± 0.1	2003.3 ± 30.8	531.8 ± 142.5	2.32 ± 0.39	1.48 ± 0.25
750 A	0–3	2097.9 ± 0.0	7.93 ± 0.09	10.53 ± 0.73	34.5 ± 0.2	2002.9 ± 28.4	663.0 ± 146.5	1.89 ± 0.34	1.20 ± 0.21
1000 A	0–3	2355.1 ± 25.7	7.81 ± 0.10	9.66 ± 0.91	34.5 ± 0.2	2297.9 ± 39.7	1003.1 ± 244.7	1.61 ± 0.33	1.02 ± 0.21
380 A+2	0–3	2357.2 ± 3.7	7.97 ± 0.09	11.84 ± 0.85	34.9 ± 0.2	2233.2 ± 31.6	679.2 ± 170.3	2.43 ± 0.39	1.55 ± 0.25
750 A+2	0–3	2402.7 ± 7.1	7.90 ± 0.09	12.04 ± 0.95	35.0 ± 0.2	2299.8 ± 30.6	815.8 ± 184.6	2.18 ± 0.37	1.39 ± 0.24
380 A	3–6	2171.7 ± 84.4	7.94 ± 0.12	11.37 ± 1.17	35.2 ± 0.2	2060.2 ± 55.2	664.7 ± 167.2	2.16 ± 0.70	1.38 ± 0.45
750 A	3–6	2090.8 ± 17.5	7.86 ± 0.10	11.60 ± 1.21	35.2 ± 0.2	2010.5 ± 48.7	790.9 ± 183.7	1.72 ± 0.42	1.10 ± 0.27
1000 A	3–6	2351.4 ± 13.3	7.75 ± 0.09	11.03 ± 0.36	35.3 ± 0.2	2302.8 ± 44.6	1136.6 ± 230.5	1.53 ± 0.35	0.98 ± 0.22
380 A+2	3–6	2361.2 ± 75.4	7.92 ± 0.09	12.85 ± 1.42	35.3 ± 0.1	2248.2 ± 96.6	771.3 ± 167.6	2.29 ± 0.46	1.47 ± 0.30
750 A+2	3–6	2238.8 ± 89.8	7.80 ± 0.10	12.84 ± 1.38	35.4 ± 0.2	2168.8 ± 107.2	990.8 ± 258.3	1.71 ± 0.41	1.09 ± 0.26
380 A	6–9	2255.2 ± 133.1	8.08 ± 0.03	15.04 ± 0.90	35.0 ± 0.1	2073.9 ± 122.9	483.0 ± 24.6	3.18 ± 0.25	2.04 ± 0.15
750 A	6–9	2183.2 ± 101.6	7.93 ± 0.09	15.66 ± 0.65	34.9 ± 0.2	2062.9 ± 131.3	722.4 ± 198.2	2.31 ± 0.32	1.49 ± 0.21
1000 A	6–9	2251.0 ± 81.7	7.79 ± 0.05	15.63 ± 0.37	34.9 ± 0.1	2176.5 ± 1.7	1028.6 ± 118.1	1.79 ± 0.19	1.15 ± 0.12
380 A+2	6–9	2111.9 ± 96.0	8.01 ± 0.07	17.93 ± 0.38	35.2 ± 0.2	1950.1 ± 109.1	568.1 ± 129.9	2.83 ± 0.38	1.83 ± 0.25
750 A+2	6–9	2170.4 ± 110.6	7.86 ± 0.11	17.90 ± 0.16	35.1 ± 0.2	2061.7 ± 140.6	871.9 ± 252.6	2.17 ± 0.47	1.40 ± 0.30
380 A	9–12	2238.0 ± 52.7	8.06 ± 0.04	13.06 ± 1.55	34.9 ± 0.1	2079.4 ± 59.8	508.3 ± 54.8	2.83 ± 0.20	1.81 ± 0.13
750 A	9–12	2228.7 ± 66.7	7.94 ± 0.07	12.89 ± 1.60	34.8 ± 0.1	2116.6 ± 69.5	694.4 ± 139.5	2.21 ± 0.29	1.41 ± 0.18
1000 A	9–12	2218.5 ± 90.6	7.78 ± 0.09	12.73 ± 1.74	34.9 ± 0.1	2157.4 ± 85.9	1015.9 ± 225.2	1.60 ± 0.29	1.02 ± 0.18
380 A+2	9–12	2165.5 ± 47.0	8.03 ± 0.06	15.55 ± 1.96	34.9 ± 0.2	2005.9 ± 38.9	536.6 ± 93.9	2.81 ± 0.30	1.81 ± 0.19
750 A+2	9–12	2164.6 ± 57.2	7.93 ± 0.08	15.63 ± 1.75	35.1 ± 0.1	2041.1 ± 62.6	694.7 ± 134.1	2.32 ± 0.33	1.50 ± 0.21

A_T, total alkalinity; Temp, temperature; DIC, dissolved inorganic carbon; Ω Ca, saturation state of calcite; Ω Ar, saturation state of aragonite.

Table 2. Characteristics and physicochemical conditions of the intertidal pools sampled for *P. lividus* sea urchins.

Tide pool	Size (m × m)	Depth (cm)	Urchins in crevices	Prevailing alga type	pH$_{NBS}$ start of the night tide	pH$_{NBS}$ end of the night tide	Mean pH$_{NBS}$ over the time course (± s.d.)	Salinity	Temperature (°C)
October 2008									
A	15 × 16	50–100	No	Erected macroalgae	8.13	7.95	8.05 ± 0.06	35.3	14.6
B	5 × 1.5	30–50	Yes	Erected macroalgae	8.10	7.70	7.89 ± 0.14	35.3	14.3
C	2.4 × 0.6	<30	Yes	Encrusting calcified algae	8.04	7.54	7.71 ± 0.18	35.4	13.9
April 2009									
A	15 × 16	50–100	No	Erected macroalgae	8.14	7.80	7.99 ± 0.12	34.7	12.8
B	5 × 1.5	30–50	Yes	Erected macroalgae	8.07	7.59	7.84 ± 0.17	34.6	12.1
C	2.4 × 0.6	<30	Yes	Encrusting calcified algae	7.84	7.40	7.59 ± 0.14	34.7	11.9

units) (Table 2). Temperature and salinity were similar in the different tide pools.

From each pool, ten individuals were collected and brought back in aerated water to the laboratory in Brussels for mechanical tests on live individuals. The mean diameter at the ambitus (mean ± s.d.) was 33.2 ± 2.7, 37.8 ± 3.4, and 34.7 ± 4.0 mm for tide pools A, B, and C, respectively. These individuals were then maintained in aquarium (recirculating system, pH_{NBS} 8.34 ± 0.01, salinity 32.2 ± 0.1, temperature 10.0 ± 0.1°C; mean ± s.d. and $n = 3$ for all parameters) for a maximum of 4 d before the mechanical tests were run.

A further ten individuals were sampled from each pool and immediately dissected, cleaned of internal organs, and dried for 48 h at 50°C for mechanical tests on individual plates. The diameter at the ambitus (mean ± s.d.) was 35.2 ± 2.7, 35.9 ± 3.3, and 33.5 ± 2.4 mm for tide pools A, B, and C, respectively. For each of these individuals, three ambital interambulacral plates and three apical interambulacral plates were analysed. Three plates of each type were also taken from three individuals per tide pool for nanoindentation measurements.

CO$_2$ seep site

To investigate the skeletal effects of natural acclimatization to a reduced pH system, adult *P. lividus* were collected from a volcanic seep gradient at Levante Bay off the island of Vulcano, Italy, in June 2013 (Calosi *et al.*, 2013b). The continuous release of CO$_2$ generates a natural pH and pCO_2 gradient along the north side of the bay

Table 3. Characteristics of the CO$_2$ seep sites sampled for *P. lividus* sea urchin (midday, 12/06/2013).

	Control site	Low pH site
pH_{NBS}	8.21	7.78
Salinity	38.2	38.1
Temperature (°C)	20.0	20.1
Total alkalinity (mmol kg$_{SW}^{-1}$)	2.545	2.506

(Boatta *et al.*, 2013; Vizzini *et al.*, 2013). Two sites were chosen: the site used as "control condition" was located 380 m away from the main CO$_2$ seeps and had a mean pH of 8.1, same as that measured for sites outside the gradients (Boatta *et al.*, 2013); the second site used as "low pH condition" was situated 300 m away from the seeps and had a mean pH of 7.8, close to predicted end-of-century values (Boatta *et al.*, 2013). This distance from the CO$_2$ seeps limited the influence of contaminants produced by the seeps, such as H$_2$SO$_4$ (Boatta *et al.*, 2013). Vizzini *et al.* (2013) showed that these sites were in "good condition" and only "moderately impacted" according to widely used pollution indices. Seawater chemistry parameters measured at the time of sea urchin collection are shown in Table 3. These are similar to results reported earlier for this location (e.g. Boatta *et al.*, 2013; Calosi *et al.*, 2013b; Vizzini *et al.*, 2013).
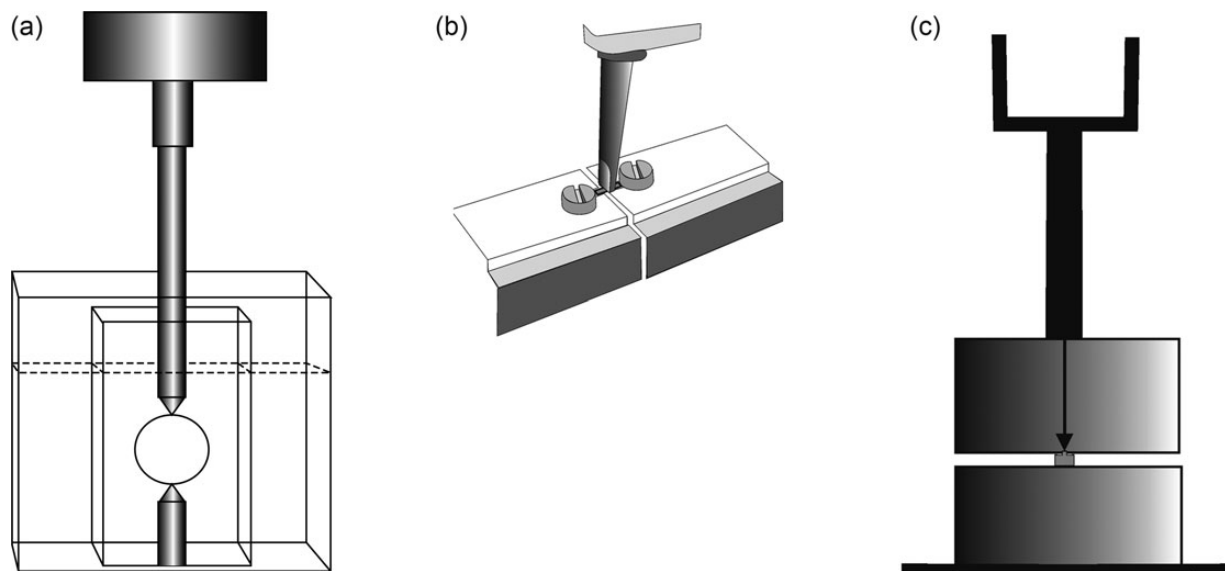
At both the control and low pH sites, three adult *P. lividus* were collected by snorkelling at a depth of 1–2 m. Urchins were then dissected, cleaned of internal organs, and dried for 48 h at 50°C. Three ambital interambulacral plates and three apical interambulacral plates from each urchin were then used for nanoindentation measurements.

Mechanical tests

To measure the fracture force of whole live individuals, a simple compression test was applied to the sea urchins. After measuring the diameter of the live sea urchins using a calliper (precision: ± 0.1 mm), the spines at the ambitus were manually removed to avoid any interference of the spines on the measurement of the test strength. The whole sea urchins were tested in a home-made device (Figure 2a) designed to mimic the jaws of a predatory fish (Guidetti and Mori, 2005). They were placed in a first container which has a perforation in the bottom part and in which acrylic plates could be inserted according to the size of the sea urchin to hold it firmly in place. This first container was placed in a second larger container filled with seawater from the aquarium at a temperature of ca. 10°C and in which was anchored a metal spike. The sea urchin was adjusted on the metal spike (which fitted through the perforation in the bottom part of the first container)

Figure 2. Schematic representation of the devices used for the mechanical tests. (a) "Jaw" device to test the strength of whole live sea urchins, (b) three-point bending stand and non-cutting blade for ambital plates, and (c) simple compression device for apical plates.

in such a way that the ambitus was balanced upon it. The mechanical test was performed using a second metal spike fixed on the load frame of a force stand (Instron 5543, Instron, Norwood, MA, USA) which was lowered at a speed of 0.35 mm min^{-1} until perforation of the test. A slow compression speed was used to avoid the rupture of the test sutures instead of the plates (Byrne *et al.*, 2014). Displacement and force were recorded continuously at a frequency of 10 Hz. Each sea urchin was tested three times, turning the sea urchin 60° each time.

All mechanical tests performed on the individual plates were carried out at room temperature (21 to 23°C). The individualized plates were cleaned of soft tissues by soaking in NaOCl 2.5% for 1.5 h and then in NaOCl 5.25% for 2.5 h; this was monitored using a dissecting microscope. In both cases, the solution was mixed frequently to immediately neutralize the lactic acid forming naturally at the surface of the skeleton during tissue digestion.

To measure the fracture force of the ambital plates, a three-point bending test was performed. The largest, and so oldest, plates were chosen. Each ambital plate was first photographed sideways in front of millimetre paper to measure the effective length (length in-between the two supporting points; see Moureaux *et al.*, 2011) and the thickness of the plates using the Image J software (Rasband, W.S., U.S. National Institutes of Health, Bethesda, MD, USA). They were then placed on a metal stand and the mechanical test was performed using a non-cutting blade fixed on the load frame of the force stand (Instron 5543) which was lowered on the primary tubercle of the plate at a speed of 0.1 mm min^{-1} (three-point bending test) until fracture (Figure 2b). Displacement and force were recorded continuously at a frequency of 10 Hz. The two halves of the plates were recovered and one was mounted on an aluminium stub, coated with gold for 4 min (JFC-1100 E ion sputter), and observed in a scanning electron microscope (JEOL JSM-6100). Digital pictures of the cross sections were recorded and subsequently used in ImageJ with the macro MomentMacro developed for the calculation of the second moment of area (I_2) (Ruff C., Johns Hopkins University School of Medicine, MD, USA) and for the measure of the plate density. I_2 is a measure of the distribution of the stereom within the plate. The density reflects the proportion of stereom in the plate fracture surface (vs. pores). The apparent Young's modulus (E_1), characterizing the material's stiffness, was calculated according to the linear-elastic beam theory:

$$I_2 = \int y^2 dA (m^4),$$
$$E_1 = \frac{F_{max} L_e^3}{48 \Delta L I_2}$$

where F_{max} is the force at fracture (N), A the area (in transverse section) (m^2), ΔL the displacement (m), L_e the effective length (m), and y the distance from the neutral plane (m) (Moureaux *et al.*, 2011).

The fracture force of the apical plates was tested using a simple compression method. The plates chosen were the smallest ones available, as they are the youngest. Each apical plate was first photographed sideways in front of millimetre paper to measure the effective length of the plates as well as the diameter of the tubercle for subsequent estimation of the area of contact using the ImageJ software. They were then placed on a metal block and the mechanical test was carried out using a second metal block fixed on the load frame of the force stand (Instron 5543) which was lowered on the tubercle of the plate at a speed of 0.3 mm min^{-1} (simple compression

test) until fracture (Figure 2c). Displacement and force were recorded continuously at a frequency of 10 Hz. All apical plates were fractured into two pieces and not crushed. To determine the Young's modulus for the apical plates, the force–displacement curves were transformed into stress–strain curves using the following equations:

$$\text{Stress}: \quad \varepsilon = \frac{\Delta L}{L_e},$$
$$\text{Strain}: \quad \sigma = \frac{F}{A}.$$

where F is the force at a time point (N), A the area of the tubercle calculated from the picture using ImageJ software (m^2), ΔL the displacement (m), and L_e the effective length (m). The E_1 is calculated as the slope between two points of the final linear part of the curve, in this case the maximum force and the 100th point before that.

$$E_1 = \frac{\sigma_{max} - \sigma_{100th\,point}}{\varepsilon_{max} - \varepsilon_{100th\,point}} (Pa).$$

Finally, nanoindentation measurements were realized to test the strength of the calcium carbonate itself. For nanoindentation analysis, the samples were embedded in epoxy resin and polished until the calcium carbonate of the skeleton was exposed at the surface. Thereafter, they were ultra-polished using sandpapers of increasing grain size (from 180 to 2400), and then with aluminium oxide. Each plate was measured once and three plates from each type from three individuals were analysed for each treatment. The nanoindentation measurements were done using a nanoindenter (TriboIndenter, Hysitron, Minneapolis, MN, USA) with a charge of 3000 μN and a Berkovich tip (a low charge was chosen to avoid any confounding effect of the resin; Presser *et al.*, 2010). The sample elastic modulus (Young's modulus; E_2) and hardness values were automatically determined from the unloading curve of the indentation test (Oliver and Pharr, 1992).

Statistical analysis

All ANOVA models were built according to the recommendations of Doncaster and Davey (2007). Data obtained from the samples of intertidal pools and CO$_2$ seeps were tested using a two-factor nested ANOVA (tide pool or site, fixed factor; sea urchin, random factor nested within tide pool or site) followed by Tukey tests for multiple comparisons. For the laboratory experiment measures, the data were regrouped under a variable named "condition" which figured the different treatments (380A, 750A, 1000A, 380A+2, and 750A+2) as using a fully crossed model was not possible due to the lack of a 1000-μatm treatment with increased temperature. Data other than nanoindentation measurements obtained from the samples of the laboratory experiment were tested using a nested cross-factored model ANOVA (condition, fixed factor; aquarium, random factor nested within condition; sea urchin, random factor nested within aquarium). The nested ANOVAs are model III ANOVAs which consider that the individuals sampled in the same tanks are not true replicates (MS of the seawater pH effect/MS of the tanks nested in seawater pH to calculate the F-ratio instead of using the MS of the model error) (Doncaster and Davey, 2007). Nanohardness measurements for the laboratory experiment were analysed using a two-factor nested ANOVA (condition, fixed factor; sea urchin, random factor nested within condition) as only one sea urchin per aquarium was used. When fracture force was significantly

correlated with length, ANCOVAs were used with size as a covariate (whole sea urchins for the tide pools, apical plates for the tide pools and the laboratory experiment, ambital plates for the laboratory experiment). All correlation analyses were carried out using simple correlations of Spearman with associated Bonferroni probabilities. All tests were realized using the software Systat 12 (Systat Software Inc., USA). Among treatment responses were also assessed using logarithmic response ratios according to the equations from Hedges *et al.* (1999) for *L* and the 95% confidence interval (CI). Results of the analysis are reported in Supplementary Figure S1.

Results
Twelve-month laboratory acclimation
A summary of the values measured and the results of the statistical analyses are presented in Table 4. There was no significant difference in the length of the ambital plates from the different treatments (condition ANOVA, $p = 0.998$) or of the apical plates (condition ANOVA, $p = 0.934$). The fracture force of the ambital plates was significantly correlated with the effective length of the plate (L_e range: $4.5-12.0$ mm; $n = 171$; $r = 0.263$, $p = 0.001$) and also to the size at the ambitus of the sea urchin (ambitus range: $29.4-54.7$ mm; $n = 171$; $r = 0.329$, $p < 10^{-3}$). For the apical plates, the fracture force was correlated with the effective length of the plates (L_e range: $1.0-3.6$ mm; $n = 171$; $r = 0.221$, $p = 0.004$) and to the size at the ambitus of the sea urchin (ambitus range: $29.4-54.7$ mm; $n = 171$; $r = 0.210$, $p = 0.006$). The mechanical properties measured

on the ambital plates and the apical plates for individuals from the five different treatments did not show any significant differences according to treatment [condition AN(C)OVA, $p \geq 0.315$]. This was confirmed by the log response ratio analysis (Supplementary Figure S1a).

Intertidal pools
A summary of the values measured and the results of the statistical analyses are presented in Table 5. There was no significant difference in the length of the ambital plates from the different tide pools (tide pool ANOVA, $p = 0.090$) or of the apical plates (tide pool ANOVA, $p = 0.400$). The fracture force of whole sea urchins was significantly correlated with size at the ambitus of the sea urchin (ambitus range: $27.2-42.7$ mm; $n = 30$; $r = 0.416$, $p = 0.022$). The force needed to break whole sea urchins did not differ significantly between the individuals from the different tide pools (tide pool ANCOVA, $p = 0.543$). This was confirmed by the log response ratio analysis (Supplementary Figure S1b).

The fracture force for the ambital plates was neither correlated with the effective length of the plate (L_e range: $4.1-7.9$ mm; $n = 90$; $r = -0.018$, $p = 0.867$) nor correlated with the size at the ambitus of the sea urchin (ambitus range: $29.4-40.2$ mm; $n = 90$; $r = -0.180$, $p = 0.089$). The fracture force needed to break the ambital plates differed significantly according to the tide pool of origin of the sea urchins (tide pool ANOVA, $p = 0.041$), with the plates from individuals of tide pool A breaking at a lower force

Table 4. Results of the different mechanical tests (mean $\pm$ s.d.) and of the statistical analyses performed on the samples from *P. lividus* sea urchins from the laboratory experiment.

Mechanical test	Mechanical property	380 A	750 A	1000 A	380 A+2	750 A+2	AN(C)OVA F	AN(C)OVA p	n
Ambital plates	F (N)	11.5 ± 3.7	12.7 ± 4.2	13.4 ± 4.3	12.4 ± 5.1	13.5 ± 4.1	0.077	0.971	10, 11, or 12
	E_1 (GPa)	11.2 ± 4.8	9.2 ± 4.3	10.9 ± 5.1	10.7 ± 6.6	8.3 ± 4.7	$<10^{-3}$	1.000	10, 11, or 12
	I_2 ($\times 10^{-13}$ m^4)	1.7 ± 1.2	1.9 ± 1.1	1.6 ± 1.1	1.6 ± 0.9	2.1 ± 1.7	1.069	0.315	10, 11, or 12
	H (GPa)	4.3 ± 0.7	4.3 ± 0.5	4.4 ± 0.7	4.1 ± 0.6	4.4 ± 0.7	0.222	0.920	3
	E_2 (GPa)	57.1 ± 10.9	57.4 ± 9.3	59.5 ± 12.1	53.4 ± 13.6	48.1 ± 20.0	0.542	0.709	3
Apical plates	F (N)	25.5 ± 9.8	26.5 ± 10.6	23.3 ± 8.4	23.9 ± 12.0	22.9 ± 9.3	$<10^{-3}$	0.994	10, 11, or 12
	E_1 (GPa)	1.3 ± 0.7	1.6 ± 1.0	1.5 ± 0.8	1.3 ± 0.7	1.6 ± 0.9	0.020	0.980	10, 11, or 12
	H (GPa)	4.6 ± 0.3	4.2 ± 0.5	4.3 ± 0.5	4.5 ± 0.6	4.3 ± 0.8	0.805	0.549	3
	E_2 (GPa)	61.7 ± 11.9	46.0 ± 16.3	54.1 ± 15.0	56.5 ± 7.2	50.1 ± 11.2	0.718	0.599	3

F, force at fracture; E_1, Young's modulus calculated from the mechanical test (three-point bending for ambital plates or simple compression for apical plates); E_2, Young's modulus obtained from nanoindentation measurements; I_2: second moment of area; *H*, hardness from nanoindentation measurements.

Table 5. Results of the different mechanical tests (mean $\pm$ s.d.) and of the statistical analyses performed on the samples from *P. lividus* sea urchins from the intertidal pools.

Mechanical test	Mechanical property	Tide pool A (low variation)	Tide pool B (intermediate)	Tide pool C (high variation)	AN(C)OVA F	AN(C)OVA p	n
Whole sea urchin	F (N)	58.1 ± 10.6	61.2 ± 14.5	51.8 ± 9.4	0.625	0.543	10
Ambital plates	F (N)	9.6 ± 3.8^a	$10.5 \pm 3.0^{a,b}$	12.6 ± 3.1^b	3.616	**0.041**	10
	E_1 (GPa)	9.1 ± 6.1	9.3 ± 6.7	6.7 ± 4.6	1.267	0.298	10
	I_2 ($\times 10^{-13}$ m^4)	1.3 ± 0.6	1.4 ± 0.9	1.4 ± 0.7	1.196	0.318	10
	H (GPa)	4.6 ± 1.3	3.7 ± 0.9	3.8 ± 0.7	3.919	0.082	3
	E_2 (GPa)	62.0 ± 8.1^a	44.6 ± 10.7^b	46.7 ± 10.4^b	11.048	**0.010**	3
Apical plates	F (N)	24.8 ± 6.9	27.5 ± 7.2	26.4 ± 7.7	0.981	0.388	10
	E_1 (GPa)	1.2 ± 0.6	1.5 ± 0.8	1.2 ± 0.7	1.378	0.269	10
	H (GPa)	4.8 ± 1.2	4.1 ± 0.8	4.3 ± 1.4	0.419	0.676	3
	E_2 (GPa)	56.1 ± 12.7	55.1 ± 12.0	58.3 ± 12.3	0.109	0.899	3

Probabilities in bold highlight a significant difference ($p < 0.05$). Means sharing the same superscript are not significantly different ($p > 0.05$). *F*, force at fracture; E_1, Young's modulus calculated from the mechanical test (three-point bending for ambital plates or simple compression for apical plates); E_2, Young's modulus obtained from nanoindentation measurements; I_2, second moment of area; *H*, hardness from nanoindentation measurements.

Table 6. Results of the different mechanical tests (mean $\pm$ s.d.) and of the statistical analyses performed on the samples from *P. lividus* sea urchins from the CO_2 seep sites.

Mechanical test	Mechanical property	Control site	Low pH site	ANOVA F	ANOVA p	n
Ambital plates	H (GPa)	3.7 $\pm$ 0.9	4.1 $\pm$ 1.0	0.535	0.505	3
	E (GPa)	44.7 $\pm$ 3.7	50.4 $\pm$ 22.4	0.195	0.682	3
Apical plates	H (GPa)	3.8 $\pm$ 0.6	3.7 $\pm$ 1.0	0.058	0.822	3
	E (GPa)	43.3 $\pm$ 8.9	38.4 $\pm$ 19.4	0.167	0.704	3

E, Young's modulus obtained from nanoindentation measurements; *H*, hardness from nanoindentation measurements.

than those from the tide pool C ($p_{\text{Tukey}} = 0.036$), whereas the forces measured for individuals of tide pool B were not different from that of any of the two other tide pools ($p_{\text{Tukey}} \geq 0.189$). The log response ratio analysis did not find any significant effect, although the force needed to break the ambital plates of sea urchins from tide pool C was on the margin of being significantly different from that of sea urchins from tide pool A ($L = 0.27$; 95% CI between -0.02 and 0.56). The Young's modulus measured via nanoindentation (E_2) showed significant differences according to the tide pool from which the sea urchins originated (tide pool ANOVA, $p = 0.010$), with those from tide pool A having significantly greater E_2 values than those from the two other tide pools ($p_{\text{Tukey}} \leq 0.012$). Those from tide pools B and C had E_2 that did not differ from each other ($p_{\text{Tukey}} = 0.856$). The difference in E_2 between sea urchins from tide pools A and B was confirmed by the log response ratio analysis ($L = -0.33$; 95% CI between -0.020 and -0.639). With this analysis, the difference in E_2 between the sea urchins of tide pools A and C was on the margin of significance ($L = -0.28$; 95% CI between 0.009 and -0.576; Supplementary Figure S1b). The modulus measured via the three-point bending method (E_1) did not show any significant difference in between the individuals from the different tide pools (tide pool ANOVA, $p = 0.298$). No other parameter measured differed significantly (tide pool ANOVA, $p \geq 0.082$). There were no significant differences in thickness of the plates (tide pool ANOVA, $p = 0.158$), which was of 0.6 ± 0.1, 0.7 ± 0.1, and 0.7 ± 0.1 mm for tide pools A, B, and C, respectively. Also, there was no significant difference in the density of the skeleton within the plates (tide pool ANOVA, $p = 0.496$), which was of 81 ± 18, 79 ± 18, and $75 \pm 24\%$ for tide pools A, B, and C, respectively.

The fracture force of the apical plates was significantly correlated with the effective length of the plate (L_e range: $1.3–2.9$ mm; $n = 88$; $r = 0.460$, $p < 10^{-3}$) but not with the size at the ambitus of the sea urchin (ambitus range: $29.4–40.2$ mm; $n = 88$; $r = 0.019$, $p = 0.857$). Apical plates from the sea urchins originating from the three tide pools showed no significant differences for any of the parameters measured [tide pool AN(C)OVA, $p \geq 0.269$]. This was confirmed by the log response ratio analysis (Supplementary Figure S1b).

CO_2 seep site
A summary of the values measured and the results of the statistical analyses are presented in Table 6. None of the nanoindentation parameters measured on the ambital and apical plates differed significantly between the individuals from the control site and those from the low pH site (site ANOVA, $p \geq 0.505$). This was confirmed by the log response ratio analysis (Supplementary Figure S1c).

Discussion
The results of this study showed that long-term (12-month) laboratory exposure to reduced pH (8.0 as control, 7.9, and 7.8) and

increased temperature ($+2°C$) had no statistically significant effect on the skeletal mechanical properties of the sea urchin *P. lividus*. Similar conclusions are drawn from the observations for sea urchins exposed to naturally constant low pH conditions at the CO_2 seep site.

However, tide pool sea urchins exposed to the most variable pH (ΔpH: -0.4 to -0.5) showed ambital plates with a significantly (although marginally) higher fracture force and a lower Young's modulus, i.e. a lower stiffness, than those from sea urchins in tide pools characterized by smaller pH fluctuations (ΔpH: -0.2). Sea urchins growing in tide pools with large pH fluctuations may experience reduced growth rates and show a modified allocation of resources. This leads to increased maintenance of the skeleton and thickening, as was shown for sea urchins living in wave exposed environments compared with those living in protected areas (Ebert, 1975). However, thickness of the plates was not significantly different for individuals from the different tide pools ($0.6–0.7$ mm). Reduced growth may also result in a density increase of the test (Smith, 1980). However, there were no significant differences in the density of the plates in-between the individuals from the different tide pools. In fact, the material properties themselves were modified, resulting in a higher flexibility. Changes in material properties according to subpopulations of *P. lividus* from the same region were also found for the spines and were correlated with differences in wave exposure (Moureaux *et al.*, 2010). This change in flexibility is probably the reason the fracture force increases: as the material composing the plate increases in flexibility, the bending tension that the plate can withstand before it breaks also increases. Depending on the energetic cost of these changes, this may lead to changes in growth rates and gonad development (e.g. Stumpp *et al.*, 2012). The sea urchins from the tide pool with the largest pH variability and showing changes of mechanical properties are on average much smaller in size than those from the other tide pools (although for this study specimens of the same size were purposely collected in each tide pool) (MC, pers. obs.). Interestingly, the tide pools harbouring sea urchins with a higher fracture force mainly contained encrusting calcifying algae, whereas the two other pools contained erected non-calcifying macroalgae (Table 2). This is reminiscent of results by Asnaghi *et al.* (2013) who showed that acidification effects on growth and skeleton strength were increased when juvenile *P. lividus* were fed non-calcifying algae compared with those fed coralline algae. This result is particularly interesting as it has been shown recently that fleshy algae are usually favoured by reduced seawater pH over crustose algae, including in rock pools (Olischläger *et al.*, 2013).

The results from the laboratory experiment and from field exposed sea urchins at the CO_2 seeps in Vulcano showed that long-term exposure to moderate seawater acidification and warming, in the range expected by 2100, did not affect the mechanical properties of the skeleton plates of *P. lividus*. This observation holds for ambital

plates but also for the apical plates which were entirely or mostly formed during the long-term experiment. This supports the short-term (6 weeks) results of Holtmann *et al.* (2013) on *Strongylocentrotus droebachiensis*. Our results also agree with observations showing that some sea urchins do survive well and calcify in waters undersaturated for aragonite and/or calcite, such as deep waters or upwelling regions, but also when their coelomic fluid is undersaturated for $CaCO_3$ (David *et al.*, 2005; Calosi *et al.*, 2013b; Collard *et al.*, 2014a, b). The lack of any temperature effect in our study may be due to the small temperature increment applied. Indeed, except for summer period (months 6–9), the sea urchins were exposed to temperatures which were within their natural seasonal range, although it should be noted that in the field such increases temperature are transitory and not chronic as in the present study. *Paracentrotus lividus* is also a eurythermal species as its distribution limits correspond more or less to the 8°C winter and 28°C summer isotherms (Boudouresque and Verlaque, 2013). Hermans *et al.* (2010) also showed that *P. lividus* juveniles maintained at temperatures ranging from 13 to 24°C did not show differences in growth rates after 6 months of exposure. This lack of a significant pH and/or temperature effect on skeletal mechanical properties might appear contradictory to the decrease in the abundance of *P. lividus* observed near CO_2 seeps (Hall-Spencer *et al.*, 2008; Calosi *et al.,* 2013b). However, the ability of the sea urchins to build their skeleton under low pH conditions does not preclude other problems such as energetic costs linked to the need of eliminating protons from the calcification site, making the seep sites not unbearable but less favourable compared with surrounding sites where the main food source, non-calcified macroalgae, is less abundant but the pH not so low (Calosi *et al.*, 2013b).

Similar mechanical results were found for the serpulid tubeworm *Hydroides elegans* for which Chan *et al.* (2013) showed no significant impact of pH on hardness (*H*) or the Young's modulus (E_2) of the worm tubes exposed to a pH of 7.8 for 17 d, the tubes were completely formed in reduced pH conditions. However, they did find a significant increase in *H* and E_2 under strongly increased temperature conditions ($\Delta T = 6$°C). For the bivalve *Arctica islandica* exposed to pH down to 7.8 for 90 d, no modifications of the shell growth rate or the shell microstructure were reported (Stemmer *et al.*, 2013). Finally, the same was observed for the barnacle *Amphibalanus improvisus* with shells exhibiting no difference in strength after exposure to a pH of 7.5 for 12 and 20 weeks and of 7.3 for 86 d (Pansch *et al.*, 2013, 2014). However, in the latter case, food availability increased the strength of the shells (Pansch *et al.*, 2014).

E_1 values measured for *P. lividus* ambital test plates ranged between 7 and 11 GPa. These values are lower than those measured previously for the spines of the same species which averaged 22 GPa (Moureaux *et al.*, 2010). This is due to differences in the shape (rectangular cuboid vs. cone) and structure (unorganized mesh structure vs. highly organized structure formed of radial septa linked by stereomic bridges) of the plates and spines (Smith, 1980; Moureaux *et al.*, 2010). Alternatively, values obtained via nanoindentation (E_2) were of 38–60 GPa and are of the same order of magnitude than those for sea urchin spines and for other marine invertebrates, analysed with the same method (Table 7). These values are much higher than E_1 values obtained via the bending test. Such a difference between E_1 and E_2 was reported previously for sea urchins (Moureaux *et al.*, 2010; Presser *et al.*, 2010) and may be explained by the method of calculation of I_2 and the anisotropic nature of the material. On the contrary, the *E* values obtained through nanoindentation (at very small indentation loads) are measured directly within the material (Presser *et al.*, 2010). This could suggest that nanoindentation is more appropriate and should be favoured when investigating the material properties. However, bending tests are more relevant on the ecological point of view as they provide the fracture forces and stiffness characteristics directly in relation to forces to which the sea urchin is submitted.

The values obtained for E_1, E_2, and *H* were all in the same range, no matter the origin of the sea urchins. The processes regulating the structure and composition of the calcite mineral are thus similar in all the different populations studied here. The values measured for both nanoindentation parameters are similar, or sometimes higher for H, to those measured in other sea urchins and some marine invertebrates (Table 7). As reported previously, the biogenic calcite produced by the sea urchins shows mechanical properties different from that of pure calcite with hardness increased by ~ 1 GPa, and stiffness reduced by ~ 20 GPa. This implies a more flexible material which is more resistant when hit for instance by pebbles displaced by waves or when facing predator attacks (Guidetti and Mori, 2005). The strength of the test of whole live sea urchins submitted to a perforation stress is on average 57 ± 5 N. Considering that the force developed by the jaw of a great barracuda (the only fish for which jaw force is available) may reach 93 N (Habegger *et al.*, 2011), the device we used in this study is well suited to replicate a fracture test in the same order of magnitude as what could be induced by the jaw of a fish: for example, that of *Diplodus sargus* or *Diplodus vulgaris*, two species of fish which turn the sea urchins upside down and attack the skeleton until it fractures (Guidetti and Mori, 2005). The fracture forces for the ambital and apical plates averaged 12 and 25 N, respectively; the difference is probably due to the different methodologies used (see the "Material and methods" section). The obtained values for the ambital plates correspond to those reported by Ellers *et al.* (1998) for the sea urchin *S. droebachiensis*, using the same method of three-point bending, which were of 12–20 N. Fracture force of apical and ambital plates was correlated with the effective length and/or to the ambital size of the sea urchin. This is probably due to changes in plate length/width during the growth of the sea urchin (Deutler, 1926). The effect of the ambital plates size was only evidenced in the laboratory experiment because of a narrower size range in the tide pool urchins, as previously reported by Ellers *et al.* (1998).

The results indicate that *P. lividus* can building a skeleton mechanically efficient when exposed to pH values close to that predicted for 2100 in laboratory and field conditions. Significant differences were only recorded between sea urchins from tide pools with different natural levels of pH fluctuation. As factors other than pH differ between these tide pools (Table 2), the observed differences cannot be attributed without ambiguity to pH alone. In fact, differences in mechanical properties of the sea urchin spines were previously reported and linked to factors such as wave exposure or food availability (Moureaux and Dubois, 2012). The effect of food availability on the capacity of organisms to build a skeleton as shown in barnacles by Pansch *et al.* (2014) and that of a calcified diet would deserve further investigation as emphasized by Asnaghi *et al.* (2013, 2014) and Moulin *et al.* (2014). Also, individuals living in very variable environments did not cope better with changes predicted to occur by the end of this century. Sea urchins studied here were sampled from very different environments and still all showed similar skeleton mechanical properties, thus confirming the validity of our general results. This is in accordance with the results of LaVigne *et al.* (2013) who found no variation in skeletal composition

Table 7. Values (mean $\pm$ s.d.) of nanohardness (H) and Young's modulus (E) measured via nanoidentation using a Berkovitch tip reported for organisms producing calcium carbonate minerals.

Group	Species	Structure	Load (μN)	H (GPa)	E (GPa)	Reference
Pure calcite			5×10^{-3}	2.4 ± 0.1	74.4 ± 2.9	Raman and Kumar (2011)
				2.7 ± 0.2	73.5 ± 2.9	Ma *et al.* (2008)
			15×10^{3}	1.9 ± 0.1	76.6 ± 1.9	Presser *et al.* (2010)
Pure dolomite				6.5 ± 0.9	117 ± 7.8	Ma *et al.* (2008)
Euechinoid	*Paracentrotus*	Spines—septa	50×10^{3}	3.8 ± 0.3	58.6 ± 3.8	Moureaux *et al.* (2010)
Sea urchin	*lividus*	Spines—central stereom	50×10^{3}	1.8 ± 0.7	32.2 ± 3.3	Moureaux *et al.* (2010)
		Ambital plates—tidal pools	3×10^{3}	4.0 ± 1.0	51.1 ± 13.7	This study
		Ambital plates—laboratory experiment	3×10^{3}	4.3 ± 0.6	55.1 ± 13.7	This study
		Ambital plates—CO_2 seeps	3×10^{3}	3.9 ± 0.9	47.6 ± 17.4	This study
		Apical plates—tidal pools	3×10^{3}	4.4 ± 1.2	56.5 ± 11.9	This study
		Apical plates—laboratory experiment	3×10^{3}	4.4 ± 0.6	53.7 ± 13.3	This study
		Apical plates—CO_2 seeps	3×10^{3}	3.8 ± 0.8	40.8 ± 14.9	This study
	Heterocentrotus mamillatus	Spine—Growth ring 1	15×10^{3}	3.7 ± 0.3	61.9 ± 2.7	Presser *et al.* (2010)
		Spine—Growth ring 2	15×10^{3}	3.4 ± 0.4	62.6 ± 3.7	Presser *et al.* (2010)
		Spine—Growth ring 3	15×10^{3}	3.5 ± 0.3	60.9 ± 4.0	Presser *et al.* (2010)
		Spine—Growth ring 4	15×10^{3}	3.4 ± 0.4	61.5 ± 3.9	Presser *et al.* (2010)
		Spine—Outer porous area	15×10^{3}	3.3 ± 0.3	50.5 ± 3.0	Presser *et al.* (2010)
		Spine—Inner porous area	15×10^{3}	3.1 ± 0.4	39.8 ± 6.1	Presser *et al.* (2010)
Cidaroid	*Phyllacanthus imperialis*	Spine—Outer porous area	15×10^{3}	4.0 ± 0.3	48.4 ± 4.2	Presser *et al.* (2010)
Sea urchin		Spine—Middle porous area	15×10^{3}	4.0 ± 0.5	46.9 ± 5.1	Presser *et al.* (2010)
		Spine—Inner porous area	15×10^{3}	2.8 ± 0.8	28.9 ± 5.8	Presser *et al.* (2010)
	Prinocidaris baculos	Spine—Porous outer part	15×10^{3}	3.9 ± 0.4	59.1 ± 5.0	Presser *et al.* (2010)
		Spine—Massive outer part (cortex)	15×10^{3}	3.5 ± 0.2	71.7 ± 3.8	Presser *et al.* (2010)
		Spine—Outer porous area	15×10^{3}	3.7 ± 0.5	52.8 ± 7.8	Presser *et al.* (2010)
		Spine—Inner porous area	15×10^{3}	3.5 ± 0.5	48.5 ± 5.7	Presser *et al.* (2010)
Serpulid tubeworm	*Hydroides elegans*	Tube	$1.5 - 7 \times 10^{3}$	$1.5 - 3$	$20 - 50$	Chan *et al.* (2013) (from Figure 3a)
Barnacle	*Amphibalanus reticulatus*	Pariete outer lamina	5×10^{-3}	3.3 ± 0.2	66.3 ± 2.7	Raman and Kumar (2011)
Oyster	*Crassostrea gigas*	Folia	5×10^{-3}	3.2 ± 0.1	73 ± 1.2	Lee *et al.* (2008)
Pteropod	*Limacina helicina antarctica*	Piece of shell	5×10^{3}	2.3 ± 0.1	45.3 ± 0.9	Teniswood *et al.* (2013)
	Cavolinia uncinata	Shell—transverse cross section	$1.2 - 1.3 \times 10^{3}$	5.2 ± 0.4	85.9 ± 2.7	Zhang *et al.* (2011)
		Shell—parallel section	$1.2 - 1.3 \times 10^{3}$	5.6 ± 0.3	51.5 ± 1.6	Zhang *et al.* (2011)

Values from this study are averages of the data from all treatments.

according to environmental conditions in adult *Strongylocentrotus purpuratus*. Because test integrity defines individual predation risk, and thus survival (unlike spines which are easily regenerated in *P. lividus*), the fact that neither the calcification nor some aspects of physiology of *P. lividus* are highly affected by ocean acidification, at least over short-term exposure (Calosi *et al.*, 2013b; Collard *et al.*, 2013, 2014b), points out that this species structural integrity, activity and survival at the adult stage should not be significantly compromised by near-future changes in ocean chemistry. However, reduced seawater pH can affect some of their primary food item (e.g. algae; Asnaghi *et al.*, 2013; Borell *et al.*, 2013; Burnell *et al.*, 2013). In fact, Asnaghi *et al.* (2013) showed that calcifying algae lose weight with an increased pCO$_2$ and that sea urchin grazing increased this phenomenon, whereas non-calcifying algae did not seem affected by reduced seawater pH. Similarly, Burnell *et al.* (2013) showed that ocean acidification and warming accentuated sea urchin grazing. The results of our study combined to those of previously published research indicate a good resistance of sea urchin skeleton to reduced seawater pH, contrarily to what was suggested. As the calcification process is intracellular in sea urchins, this is not so surprising as the calcification fluid composition may be biologically controlled.

Authors' contributions

MC was responsible for the original concept and was supported in the development of the concept by PD, SPSR, and FD. MC also analysed all the data and wrote the manuscript. Test samples from the lab experiment were collected and prepared by MC and SPSR, with the water chemistry analysed by HSF, supported by PC and SW. Test samples from the tide pools were collected and prepared by MC and YD, supported by LM. Test samples from the CO$_2$ seep site were collected and prepared by SPSR supported by MM and JMH-S. The analysis of the mechanical properties of the test samples was carried out by MC and YD supported by PD and JD. All the authors contributed to the final manuscript.

Supplementary data

Supplementary material is available at the *ICESJMS* online version of the manuscript.

Acknowledgements

References

Asnaghi, V., Chiantore, M., Mangialajo, L., Gazeau, F., Francour, P., Alliouane, S., and Gattuso, J. P. 2013. Cascading effects of ocean acidification in a rocky subtidal community. PLoS One, 8: e61978.

Asnaghi, V., Mangialajo, L., Gattuso, J. P., Francour, P., Privitera, D., and Chiantore, M. 2014. Effects of ocean acidification and diet on thickness and carbonate elemental composition of the test of juvenile sea urchins. Marine Environmental Research, 93: 78–84.

Boatta, F., D'Alessandro, W., Gagliano, A. L., Liotta, M., Milazzo, M., Rodolfo-Metalpa, R., Hall-Spencer, J. M., *et al.* 2013. Geochemical survey of Levante Bay, Vulcano Island (Italy), a natural laboratory for the study of ocean acidification. Marine Pollution Bulletin, 73: 485–494.

Boudouresque, C. F., and Verlaque, M. 2013. *Paracentrotus lividus. In* Sea Urchins: Biology and Ecology. Developments in Aquaculture and Fisheries Science, 3rd edn, 38, pp. 297–327. Ed. by J. M. Lawrence. Elsevier, London, UK. 531 pp.

Borell, E. M., Steinke, M., and Fine, M. 2013. Direct and indirect effects of high pCO_2 on algal grazing by coral reef herbivores from the Gulf of Aqaba (Red Sea). Coral Reefs, 32: 937–947.

Burnell, O. W., Russell, B. D., Irving, A. D., and Connell, S. D. 2013. Eutrophication offsets increased sea urchin grazing on seagrass caused by ocean warming and acidification. Marine Ecology Progress Series, 485: 37–46.

Byrne, M., Smith, A., West, S., Collard, M., Dubois, P., Graba-landry, A., and Dworjanyn, S. 2014. Warming influences Mg^{2+} content, while warming and acidification influence calcification and test strength of a sea urchin. Environmental Science and Technology, 48: 12620–12627.

Caldeira, K., and Wickett, M. 2003. Anthropogenic carbon and ocean pH. Nature, 425: 365.

Calosi, P., Rastrick, S. P. S., Graziano, M., Thomas, S. C., Baggini, C., Carter, H. A., Hall-Spencer, J. M., *et al.* 2013b. Distribution of sea urchins living near shallow water CO_2 vents is dependent upon species acid-base and ion-regulatory abilities. Marine Pollution Bulletin, 73: 470–484.

Calosi, P., Rastrick, S. P. S., Lombardi, C., de Guzman, H. J., Davidson, L., Jahnke, M., Giangrande, A., *et al.* 2013a. Adaptation and acclimatization to ocean acidification in marine ectotherms: an *in situ* transplant experiment with polychaetes at a shallow CO_2 vent system. Philosophical Transactions of the Royal Society, Series B, 368: 20120444.

Chan, V. B., Thiyagarajan, V., Lu, X. W., Zhang, T., and Shich, K. 2013. Temperature dependent effects of elevated CO_2 on shell composition and mechanical properties of *Hydroides elegans*: insights from a multiple stressor experiment. PLoS One, 8: e78945.

Collard, M., De Ridder, C., David, B., Dehairs, F., and Dubois, P. 2014a. Could the acid-base status of Antarctic sea urchins indicate a better-than-expected resilience to near-future ocean acidification? Global Change Biology, doi:10.1111/gcb.12735.

Collard, M., Dery, A., Dehairs, F., and Dubois, P. 2014b. Euechinoidea and Cidaroidea respond differently to ocean acidification. Comparative Biochemistry and Physiology Part A, 174: 45–55.

Collard, M., Laitat, K., Moulin, L., Catarino, A., Grosjean, P., and Dubois, P. 2013. Buffer capacity of the coelomic fluid in echinoderms. Comparative Biochemistry and Physiology Part A, 166: 199–206.

David, B., Choné, T., Mooi, R., and De Ridder, C. 2005. Antarctic Echinoidea. Synopses of the Antarctic Benthos, 10. Koeltz Scientific Books, Königstein, 274 pp.

Dery, A., Guibourt, V., Catarino, A. I., Compère, P., and Dubois, P. 2014. Properties, morphogenesis, and effect of acidification on spines of the cidaroid sea urchin *Phyllacanthus imperialis*. Invertebrate Biology, 133: 188–199.

Deutler, F. 1926. Uber das wachstum des seeigelskeletts. Zoologische Jahrbuecher Abteilung fuer Anatomie und Ontogenie der Tiere, 48: 119–200.

Doncaster, C. P., and Davey, A. J. 2007. Analysis of Variance and Covariance. Cambridge University Press, Cambridge, UK, 287 pp.

Dubois, P. 2014. The skeleton of postmetamorphic echinoderms in a changing world. Biological Bulletin, 226: 223–236.

Dubois, P., and Chen, C. P. 1989. Calcification in echinoderms. *In* Echinoderm Studies, 3, pp. 55–136. Ed. by M. Jangoux, and J. M. Lawrence. Balkema, Rotterdam, The Netherlands, 383 pp.

Dupont, S., Dorey, N., Stumpp, M., Melzner, F., and Thorndyke, M. 2013. Long-term and trans-life-cycle effects of exposure to ocean acidification in the green sea urchin *Strongylocentrotus droebachiensis*. Marine Biology, 160: 1835–1843.

Ebert, T. A. 1975. Growth and mortality of post-larval echinoids. The American Society of Zoologists, 15: 755–775.

Ellers, O., Johnson, A. S., and Moberg, P. E. 1998. Structural strengthening of urchin skeletons by collagenous sutural ligaments. Biological Bulletin, 195: 135–144.

Findlay, H. S., Beesley, A., Dashfield, S., McNeill, C. L., Nunes, J., Queirós, A. M., and Woodward, E. M. S. 2013. UKOA Benthic Consortium, PML intertidal mesocosm experimental environment dataset. British Oceanographic Data Centre - Natural Environment Research Council, UK.

Findlay, H. S., Kendall, M. A., Spicer, J. I., Turley, C., and Widdicombe, S. 2008. Novel microcosm system for investigating the effects of elevated carbon dioxide and temperature on intertidal organisms. Aquatic Biology, 3: 51–62.

Guidetti, P., and Mori, M. 2005. Morpho-functional defences of Mediterranean sea urchins, *Paracentrotus lividus* and *Arbacia lixula*, against fish predators. Marine Biology, 147: 797–802.

Habegger, M. L., Motta, P. J., Huber, D. R., and Deban, S. M. 2011. Feeding biomechanics in the great barracuda during ontogeny. Journal of Zoology, 283: 63–72.

Hall-Spencer, J. M., Rodolfo-Metalpo, R., Martin, S., Ransome, E., Fine, M., Turner, S. M., Rowley, S. J., *et al.* 2008. Volcanic carbon dioxide vents show ecosystem effects of ocean acidification. Nature, 454: 96–99.

Hedges, L. V., Gurevitch, J., and Curtis, P. S. 1999. The meta-analysis of response ratios in experimental ecology. Ecology, 80: 1150–1156.

Hermans, J., Borremans, C., Willenz, P., André, L., and Dubois, P. 2010. Temperature, salinity and growth rate dependences of Mg/Ca and Sr/Ca ratios of the skeleton of the sea urchin *Paracentrotus lividus* (Lamarck): an experimental approach. Marine Biology, 157: 1293–1300.

Holtmann, W. C., Stumpp, M., Gutowska, M., Syré, S., Himmerkus, N., Melzner, F., and Bleich, M. 2013. Maintenance of coelomic fluid pH in sea urchins exposed to elevated CO_2: the role of body cavity epithelia and stereom dissolution. Marine Biology, 160: 2631–2645.

IPCC. 2013. Climate Change 2013: The physical science basis. *In* Contribution of Working Group I to the Fifth Assessment Report of the Intergovernmental Panel on Climate Change. Ed. by T. F. Stocker, D. Qin, G. K. Plattner, M. Tignor, S. K. Allen, J.

Boschung, A. Nauels, Y. Xia, V. Bex, and P. M. Midgley. Cambridge University Press, Cambridge, New York, NY, USA, UK.

Kitidis, V., Hardman-Mountford, N. J., Litt, E., Brown, I., Cummings, D., Hartman, S., Hydes, D., *et al.* 2012. Seasonal dynamics of the carbonate system in the Western English Channel. Continental Shelf Research, 42: 30–40.

Kurihara, H., Yin, R., Nishihara, G. N., Soyano, K., and Ishimatsu, A. 2013. Effect of ocean acidification on growth, gonad development and physiology of the sea urchin *Hemicentrotus pulcherrimus*. Aquatic Biology, 18: 281–292.

LaVigne, M., Hill, T. M., Sanford, E., Gaylord, B., Russell, A. D., Lenz, E. A., Hosfelt, J. D., *et al.* 2013. The elemental composition of purple sea urchin (*Strongylocentrotus purpuratus*) calcite and potential effects of pCO_2 during early life stages. Biogeosciences, 10: 3465–3477.

Lee, S. W., Kim, G. H., and Shoi, C. S. 2008. Characteristic crystal orientation of folia in oyster shell, *Crassostrea gigas*. Materials Science and Engineering C, 28: 258–263.

Ma, Y., Cohen, S. R., Addadi, L., and Weiner, S. 2008. Sea urchin tooth design: an "all-calcite" polycrystalline reinforced fiber composite for grinding rocks. Advanced Materials, 20: 1555–1559.

McDonald, M. R., McClintock, J. B., Amsler, C. D., Rittschof, D., Angus, R. A., Orihuela, B., and Lutostanki, K. 2009. Effects of ocean acidification over the life history of the barnacle *Amphibalanus amphitrite*. Marine Ecology Progress Series, 385: 179–187.

Melatunan, S., Calosi, P., Rundle, S. D., Widdicombe, S., and Moody, A. J. 2013. Effects of ocean acidification and elevated temperature on shell plasticity and its energetic basis in an intertidal gastropod. Marine Ecology Progress Series, 472: 155–168.

Morse, J. W., Andersson, A. J., and Mackenzie, F. T. 2006. Initial response of carbonate-rich shelf sediments to rising atmospheric pCO_2 and "ocean acidification": role of high Mg-calcites. Geochimica and Cosmochimica Acta, 70: 5814–5830.

Moulin, L., Catarino, A., Claessens, T., and Dubois, P. 2011. Effects of seawater acidification on early development of the intertidal sea urchin *Paracentrotus lividus* (Lamarck 1816). Marine Pollution Bulletin, 62: 48–54.

Moulin, L., Grosjean, P., Leblud, J., Batigny, A., and Dubois, P. 2014. Impact of elevated pCO_2 on acid-base regulation of the sea urchin *Echinometra mathaei* and its relation to resistance to ocean acidification: a study in mesocosms. Journal of Experimental Marine Biology and Ecology, 457: 97–104.

Moureaux, C., and Dubois, P. 2012. Plasticity of biometrical and mechanical properties of *Echinocardium cordatum* spines according to environment. Marine Biology, 159: 471–479.

Moureaux, C., Pérez-Huerta, A., Compère, P., Zhu, W., Leloup, T., Cusack, M., and Dubois, P. 2010. Structure, composition and mechanical relations to function in sea urchin spine. Journal of Structural Biology, 170: 41–49.

Moureaux, C., Simon, J., Mannaerts, G., Catarino, A., Pernet, P., and Dubois, P. 2011. Effects of field contamination by metals (Cd, Cu, Pb, Zn) on biometry and mechanics of echinoderm ossicles. Aquatic Toxicology, 105: 698–707.

Olischläger, M., Bartsch, I., Gutow, L., and Wiencke, C. 2013. Effects of ocean acidification on growth and physiology of *Ulva lactuca* (Chlorophyta) in a rockpool-scenario. Phycological Research, 61: 180–190.

Oliver, W. C., and Pharr, G. M. 1992. An improved technique for determining hardness and elastic modulus using load and displacement sensing indentation experiments. Journal of Materials Research, 7: 1564–1583.

Orr, J. C. 2011. Recent and future changes in ocean carbonate chemistry. *In* Ocean Acidification, pp. 41–66. Ed. by J. P. Gattuso, and L. Hansson. Oxford University Press, NY, USA. 326 pp.

Pansch, C., Nasrolahi, A., Appelhans, Y., and Whal, M. 2013. Tolerance of juvenile barnacles (*Amphibalanus improvisus*) to warming and elevated pCO_2. Marine Biology, 160: 2023–2035.

Pansch, C., Schaub, I., Havenhand, J., and Wahl, M. 2014. Habitat traits and food availability determine the response of marine invertebrates to ocean acidification. Global Change Biology, 20: 765–777.

Presser, V., Gerlach, K., Vohrer, A., Nickel, K. G., and Dreher, W. F. 2010. Determination of the elastic modulus of highly porous samples by nanoindentation: a case study on sea urchin spines. Journal of Materials Science, 45: 2408–2418.

Queiros, A. M., Fernandes, J. A., Faulwetter, S., Nunes, J., Rastrick, S. P. S., Mieszkowska, N., Artioli, Y., *et al.* 2014. Scaling up experimental ocean acidification and warming research: from individuals to the ecosystem. Global Change Biology, 21: 130–143.

Raman, S., and Kumar, R. 2011. Construction and nanomechanical properties of the exoskeleton of the barnacle *Amphibalanus reticulatus*. Journal of Structural Biology, 176: 360–369.

Rodolfo-Metalpa, R., Houlbrèque, F., Tambutté, E., Boisson, F., Baggini, C., Patti, F. P., Jeffree, R., *et al.* 2011. Coral and mollusc resistance to ocean acidification adversely affected by warming. Nature Climate Change, 1: 308–312.

Smith, A. 1980. Stereom microstructure of the echinoid test. Palaeontology, 25: 1–81.

Sokolov, A. P., Stone, P. H., Forest, C. E., Prinn, R., Sarofim, M. C., Webster, M., Paltsev, S., *et al.* 2009. Probabilistic forecast for twenty-first-century climate based on uncertainties in emissions (without policy) and climate parameters. Journal of Climate, 22: 5175–5204.

Stemmer, K., Nehrke, G., and Brey, T. 2013. Elevated CO_2 levels do not affect the shell structure of the bivalve *Arctica islandica* from the Western Baltic. PLoS One, 8: e70103.

Stumpp, M., Trübenbach, K., Brennecke, D., Hu, M. Y., and Melzner, F. 2012. Resource allocation and extracellular acid-base status in the sea urchin *Strongylocentrotus droebachiensis*. Aquatic Toxicology, 110–111: 194–207.

Teniswood, C. M., Roberts, D., Howard, W. R., and Bradby, J. E. 2013. A quantitative assessment of the mechanical strength of the polar pteropod *Limacina helicina antarctica* shell. ICES Journal of Marine Science, 70: 1499–1505.

Trousset, J. 1885. Nouveau dictionnaire encyclopédique universel illustré: répertoire des connaissances humaines. Volume 4, p. 372.

Vizzini, S., Di Leonardo, R., Costa, V., Tramati, C. D., Luzzu, F., and Mazzola, A. 2013. Trace element bias in the use of CO_2 vents as analogues for low pH environments: Implications for contamination levels in acidified oceans. Estuarine, Coastal and Shelf Science, 134: 19–30.

Welladsen, H. M., Southgate, P. C., and Heimann, K. 2010. The effects of exposure to near-future levels of ocean acidification on shell characteristics of *Pinctada fucata* (Bivalvia: Pteriidae). Molluscan Research, 30: 125–130.

Wolfe, K., Dworjanyn, S. A., and Byrne, M. 2013. Effects of ocean warming and acidification on survival, growth and skeletal development in the early benthic juvenile sea urchin (*Heliocidaris erythrogramma*). Global Change Biology, 19: 2698–2707.

Zhang, T., Ma, Y., Chen, K., Kunz, M., Tamura, N., Qiang, M., Xu, J., *et al.* 2011. Structure and mechanical properties of a pteropod shell consisting of interlocked helical aragonite nanofibers. Angewandte Chemie International Edition, 50: 10361–10365.

Ziveri, P., Passaro, M., Incarbona, A., Milazzo, M., Rodolfo-Metalpa, R., and Hall-Spencer, J. M. 2014. Decline in coccolithophore diversity and impact on coccolith morphogenesis along a natural CO_2 gradient. Biological Bulletin, 226: 282–290.